UDK 669.148:66.040.2:66.094.3
Original scientific article/Izvirni znanstveni članek

ISSN 1580-2949
MTAEC9, 53(5)705(2019)

OXIDATION BEHAVIOR OF HT9 STEEL IN 700 °C – 900 °C STEAM

OKSIDACIJA JEKLA HT9 V VODNI PARI S TEMPERATURO MED 700 °C IN 900 °C

Huayu Zhang[1], Huiqin Chen[1*], Mengmeng Zhao[2], Rui Tang[3]

[1]School of Materials Science and Engineering, Taiyuan University of Science and Technology, Taiyuan 030024, China
[2]School of Materials Science, Northwestern Polytechnical University, Xi'an 710072, China
[3]Science and Technology on Reactor Fuel and Materials Laboratory, Nuclear Power Institute of China, Chengdu 610213, China

Prejem rokopisa – received: 2019-01-31; sprejem za objavo – accepted for publication: 2019-04-11

doi:10.17222/mit.2019.030

Oxidation behavior of the HT9 steel exposed to 700 °C –900 °C steam was investigated with gravimetry, X-ray diffraction and scanning electron microscopy. It was found that the oxidation kinetics of the HT9 steel followed the parabolic law. The mass gain increased with a decreasing temperature. The steam oxidation of the HT9 steel at 800 °C and 900 °C was selective. The oxides formed on the HT9-steel surface displayed a double-layer structure, consisting of an outer columnar Fe_2O_3 layer and an inner $(Fe, Cr)_3O_4$ layer.

Keywords: HT9 steel, steam oxidation, oxidation mechanisms

Avtorji so raziskovali oksidacijo jekla HT9 izpostavljenega vodni pari, ki je imela od 700 °C do 900 °C. Raziskavo so izvajali z gravimetrijo, rentgensko difrakcijo in vrstično elektronsko mikroskopijo. Ugotovili so, da kinetika oksidacije poteka v skladu s paraboličnim zakonom. Prirastek na masi je naraščal s padajočo temperaturo. Oksidacija jekla HT9 pri 800 °C in 900 °C je bila selektivna. Oksidi nastali na površini jekla HT9, imajo dvoplastno strukturo, sestavljeno iz zunanjega stebričastega sloja Fe_2O_3 in notranjega $(Fe, Cr)_3O_4$ sloja.

Ključne besede: jeklo HT9, oksidacija z vodno paro, mehanizmi oksidacije

1 INTRODUCTION

With the depletion of traditional energy and the increasing environmental pollution, the nuclear energy plays a more important role to satisfy the urgent energy demand.[1]

To guarantee the safety of a nuclear generator, fuel cladding materials are required to withstand the extreme working conditions, such as high temperature, high pressure, strong radiation and strong corrosion.[2–6] With the advantages of good resistance to a high radiation dose, high thermal conductivity, high creep-rupture strength, and excellent oxidation and corrosion resistance at high temperatures, the HT9 steel has a great potential for the application in the components of nuclear reactors.[4,7]

In steam environments, about 9–12 % Cr ferritic steels exhibit an anomalous temperature dependence of the oxidation behavior.[8,9] Several studies indicate that multilayered oxide layers are formed on 9–12 % Cr ferritic/martensitic steels in steam atmospheres. Moreover, some defects, such as pores, voids and cracks, are present in the oxide layer.[9–13] The microstructures of the oxide and defects within the oxide layers depend on the exposure temperature and time.[8–10,14–17] Therefore, it is important to evaluate the oxidation behavior in the high-temperature steam for the nuclear fuel cladding materials.[10,18] When the supply of a nuclear reactor coolant is insufficient, the temperature of the fuel cladding of nuclear reactors rises rapidly. After severe loss-of-coolant accidents (LOCAs), a large temperature increase would lead to severe oxidation of the fuel cladding of nuclear reactors.[19] If the cladding tube cannot maintain its structural integrity, the release of radio nuclides into the environment causes a catastrophic accident. In order to improve the safety and reliability of a nuclear reactor, it is necessary to evaluate the steam-oxidation resistance of the HT9 steel.

In the present work, the steam-oxidation properties of the HT9 steel were investigated at (700, 800 and 900) °C. The weight gain and thickness of the oxide layers were utilized to characterize the oxidation properties. The morphology, chemical composition and microstructure of the oxides were studied to reveal the oxidation mechanisms.

2 EXPERIMENTAL PART

HT9-steel cladding is provided by the Nuclear Power Institute of China. The chemical composition of the HT9 steel is shown in **Table 1**. **Figure 1** displays a TEM image of the HT9 steel, which consisted of tempered martensite and $M_{23}C_6$ carbides. Carbides are precipitated

*Corresponding author's e-mail:
hyzhang76@tyust.edu.cn (H. Zhang), chenhuiqin@tyust.edu.cn (H. Chen)

at the martensitic lath and prior austenite boundaries. The size of specimens was (10 × 10 × 0.6) mm. Prior to the oxidation experiment, the specimens were ground with SiC abrasive paper of up to 1200 grit, cleaned with ethanol and weighed using a balance (FA/JA*B) with an accuracy of 0.1 mg. The steam-oxidation experiments were performed in a tube furnace. Steam was produced by ebullition of deionized water and it flowed continuously into the furnace at atmospheric pressure. The water-vapor flow rate was 10 g/min. The test temperatures were (700, 800 and 900) °C, respectively. The specimens were tested at different exposure times of up to 100 h. The weight variations of the specimens were recorded at prescribed experiment intervals. The microstructure of the as-received HT9 steel was studied with a transmission electron microscope (TEM, Tecnia F30). The cross-section of the specimens was ground and polished, and further observed with a scanning electron microscope (SEM, TESCAN MIRA3). The compositions of the oxide products were determined with an energy dispersion X-ray spectroscope (EDX, Genesis XM) attached to SEM. The structures of the oxides were studied with an X-ray diffractometer (XRD, X'pert Pro).

Table 1: Chemical composition of the HT9 steel (*w*/%)

Element	C	Mn	Si	Cr	Mo	W	V	Ni	N	Fe
Amount	0.2	0.69	0.32	11.4	1.02	0.48	0.28	0.54	0.45	bal.

3 RESULTS

3.1. Oxidation kinetics

Figure 2 shows the variation of the weight gain of the HT9 steel with the oxidation time. It is found that the weight gain increased with the increasing exposure time and decreased as the temperature increases. In good agreement with the previous results,[8,17] this phenomenon suggests that the steel has improved its resistance to steam oxidation at high temperatures. Plots are also

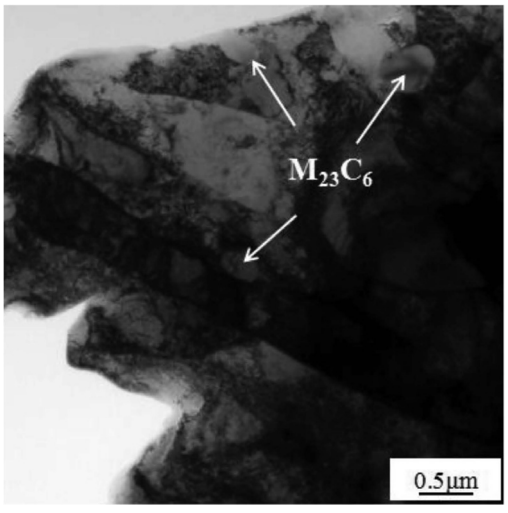

Figure 1: TEM image of the as-received HT9 steel

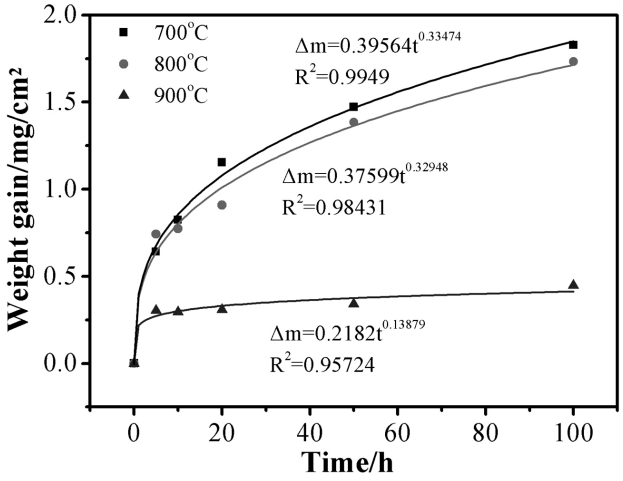

Figure 2: Weight gain of the HT9 steel as a function of exposure time at (700, 800 and 900) °C in steam

shown in **Figure 1** and can be fitted with Equation (1):[3,6,10,16,18]

$$\Delta m = kt^n \quad (1)$$

where Δm is the weight gain per unit area in mg/cm^2, k is the oxidation rate constant in mg/(cm^2 h^n), t is the time in h, and n is the time exponent.

The oxidation kinetics of the HT9 steel at (700, 800 and 900) °C followed the parabolic law. It can be calculated that the time exponents n are 0.33474 at 700 °C, 0.32948 at 800 °C and 0.13879 at 900 °C. The k values at (700, 800 and 900) °C are: 0.39564, 0.37599 and 0.21820, respectively. The highest k at the lowest temperature indicates that the HT9 steel displays the highest oxidation resistance at 900 °C.

3.2. Surface morphology

Figure 3 shows SEM images of the oxides on the HT9 steel after 100 h in 800 °C and 900 °C steam. The oxidation of the HT9 steel in steam is not uniform. Many separate cellular oxides (**Figure 3a**) appear on the surface of the HT9 steel at 800 °C. The pox-like morphology means that the steam oxidation is selective rather than uniform. At 900 °C, cellular or flaky oxides can be found on the surface of oxidized steel. In addition, the grinding scratches can be observed, as shown in **Figure 3b**. By comparing the morphologies of the oxides, it can be found that the oxidation was more serious at the lower temperature, in agreement with the results from **Figure 2**.

Figure 4 displays surface morphologies of the HT9 steel oxidized at (700, 800 and 900) °C. It can be found that the spherical oxides develop a flocculent or needle-like shape at 700 °C with the increasing exposure time, as shown in **Figures 4a** and **4b**. At 800 °C and after 50 h, the oxide particles become larger and a flake sub-structure can be observed, as shown in **Figures 4c** and **4d**. The flake sub-structure further grows with the

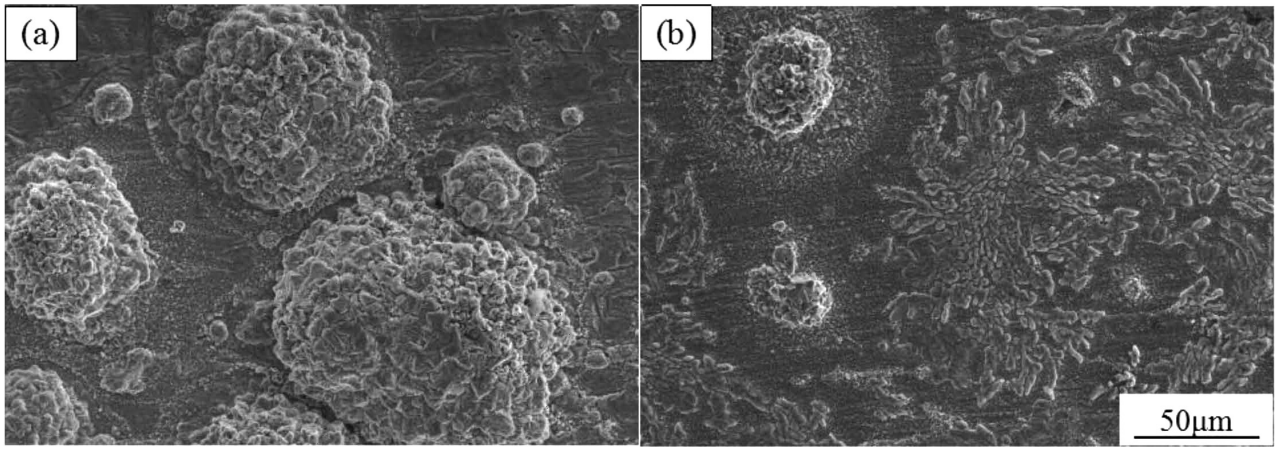

Figure 3: SEM images of the oxide films on the HT9 steel exposed to steam for 100 h: a) 800 °C, b) 900 °C

oxidation time. The evolutions of the morphology at 800 °C and 900 °C were similar. However, the oxide film had a cellular structure at 900 °C, and each cell was composed of many small crystal blocks, as shown in **Figures 4e** and **4f**. Moreover, obvious cracks could be seen on the oxide film, as shown in **Figure 4f**.

3.3. Cross-sectional microstructure

Figures 5a to **5f** display cross-sectional microstructures of the HT9 steel exposed to (700, 800 and 900) °C steam. 700 °C and 800 °C oxides are composed of two different layers, that is, a compact outer layer and a loose inner layer. Some cracks and voids are present in the oxide layers. The voids may coalesce into a crack after a long exposure time.[9,11] Crack propagation leads to an exfoliation of the oxide layer. A breakdown of the oxide films can be seen in some regions. Both layers grow with the exposure time. Similarly, double oxide layers are also found at 800 °C and 900 °C. The outer oxide layer contains columnar grains perpendicular to the surface, shown in **Figure 5c**. **Figures 5e** and **5f** show images of the cross-section of the HT9 steel at 900 °C. Localized corrosion products can be found. These phenomena indicate that a selective steam-oxidation behavior takes place at 900 °C, like in the previous studies.[17–20] Selective oxides also include two layers. The cracks between the outer/inner layers and inner layers/steel cause the exfoli-

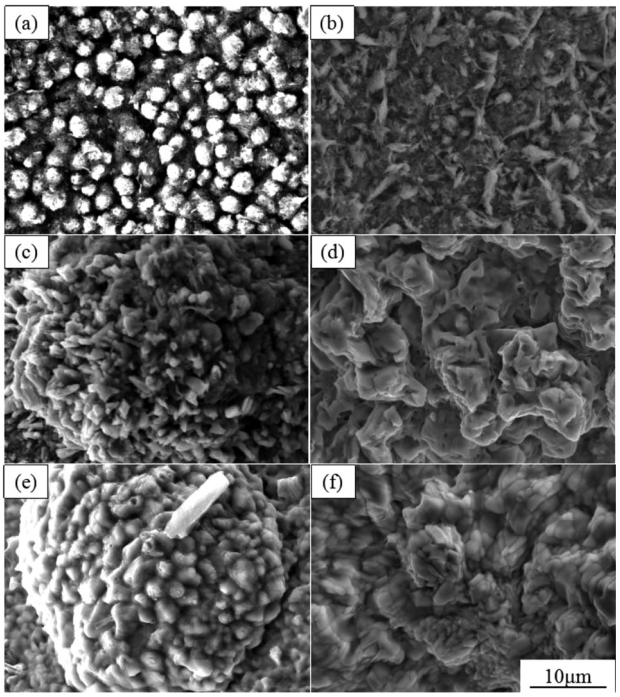

Figure 4: Surface morphologies of the oxidized HT9 steel: a) 700 °C, 50 h, b) 700 °C, 100 h, c) 800 °C, 50 h, d) 800 °C, 100 h, e) 900 °C, 50 h and f) 900 °C, 100 h

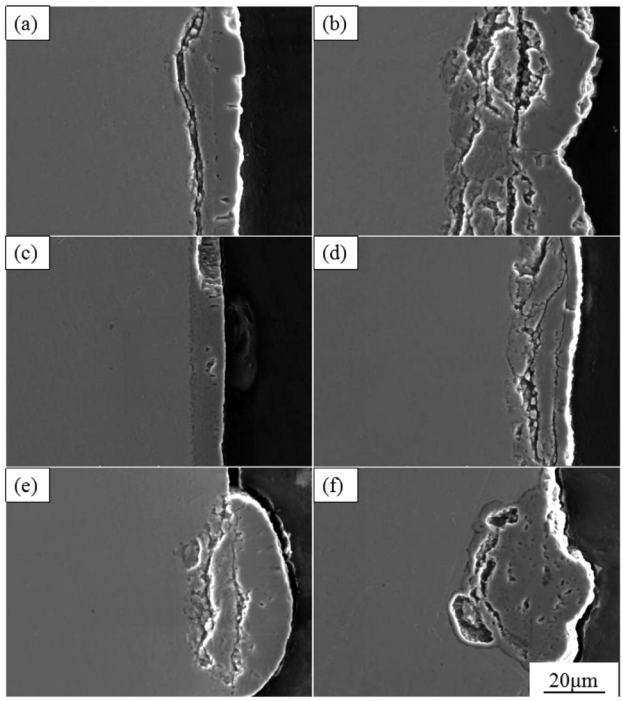

Figure 5: Cross-sectional SEM images of the HT9 steel: a) 700 °C, 10 h, b) 700 °C, 100 h, c) 800 °C, 10 h, d) 800 °C, 100 h, e) 900 °C, 5 h and f) 900 °C, 100 h

ation phenomenon, as shown in **Figure 5f**. Sometimes, debonding of the outer layer makes it peel off from the inner layer.

Figure 6 shows SEM images of cross-sections and elemental distribution of the oxide films on the HT9 steel exposed to steam. It shows that the outer layer contains Fe and O and the inner layers are rich in Fe and Cr. The O content is almost the same in the outer and inner oxide layer. The inner layer is determined as Fe-Cr spinel, in which the Cr content is higher than that in steel, and the Fe content is lower than in steel and the outer layer. To further confirm the composition of the oxides, six points in the cross-section were examined with EDS; they are listed in **Table 2**. The metal-to-oxygen ratio (M/O) for points 1, 2, 3, 4, 5 and 6 are 0.66, 0.77, 0.68, 0.76, 0.68 and 0.75, respectively. M/O in the outer layer is close to 0.67, consistent with that of Fe_2O_3. M/O in the inner layer is about 0.75 and consistent with $(Fe, Cr)_3O_4$.

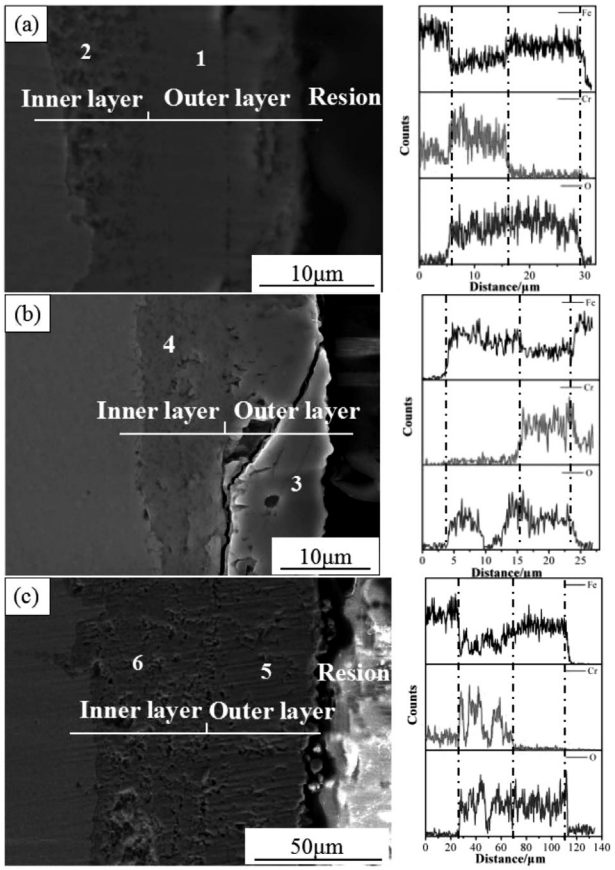

Figure 6: Cross-sectional SEM images and elemental distribution of the oxide layers on the HT9 steel exposed to steam: a) 700 °C, 100 h, b) 800 °C, 50 h and c) 900 °C, 50 h

Table 2: EDS results corresponding to the points on the cross-section from **Figure 6** (*a*/%).

Element Point	Fe	Cr	O	M/O
1	39.58	—	60.42	0.66
2	30.97	12.40	56.63	0.77
3	40.63	—	59.37	0.68
4	24.24	18.80	56.96	0.76
5	40.52	—	59.48	0.68
6	30.82	12.11	57.06	0.75

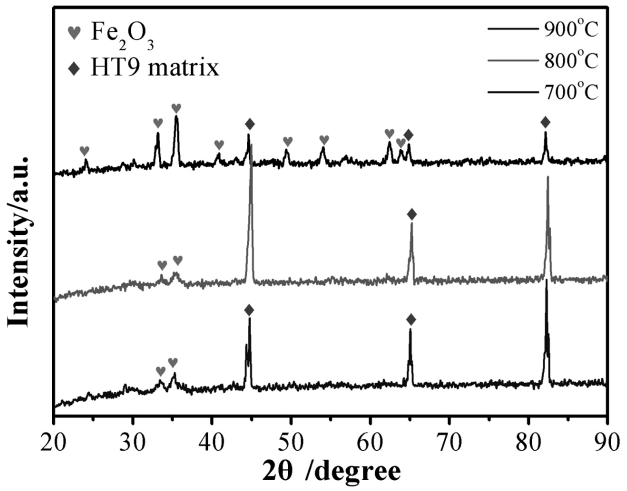

Figure 7: XRD patterns of the HT9 steel tested in a steam atmosphere for 100 h

3.4 XRD analysis

Figure 7 shows XRD patterns of the outer-layer oxide film formed on the HT9 steel exposed to steam oxidization for 100 h between 700 °C and 900 °C. Fe_2O_3 and the HT9 matrix are present. The reasons for this may be the facts that the steam oxidation of the HT9 steel was selective and the outer oxide layer was so thick that the inner Fe-Cr spinel oxide could not be detected. The decreasing intensity of Fe_2O_3 with the increasing temperature means that the amount of Fe_2O_3 reduces at the higher temperature. In other words, the steam oxidation was more serious at the lower temperature and the outer layer was Fe_2O_3, indicating s superior resistance to steam oxidation of HT9 at the higher temperature.

4 DISCUSSION

The above results indicate that the steam oxidation kinetics of the HT9 steel followed the parabolic law at the temperatures between 700 °C and 900 °C, suggesting that the oxide has a protective effect. Moreover, the steam oxidation of the HT9 steel was localized and a higher resistance to steam oxidation was observed at the higher temperature. A double-layer oxide, composed of the Fe_2O_3 outer layer and $(Fe, Cr)_3O_4$ inner layer, can be generated on the HT9 steel in 700–900 °C steam, which is similar to the results for the HT9 steel exposed to supercritical water.[14,16]

As the oxygen affinity for Cr is higher than that for Fe, Cr is more likely to be oxidized to Cr_2O_3 at the initial stage of oxidation.[10,14,21] The Cr content is not high enough to form a complete oxide layer; thus, discrete

Cr_2O_3 forms at the metal/steam interface according to Equation (2), leading to a Cr depletion in the metal substrate. Therefore, the Cr content in the inner oxide layer is higher than that in the steel substrate, as shown in **Figure 6**. The diffusion coefficient of Fe is higher than that of Cr in both oxide and metal matrix. Iron diffuses to the oxide/steam interface and reacts with H_2O following Equation (3). It is known that iron oxide is more easily reduced by hydrogen than chromium. Fe_3O_4 is reduced to Fe according to Equation (4). Then, Fe reacts with Cr_2O_3 and steam through Equation (5). Fe_3O_4 is oxidized to Fe_2O_3 at the oxide/steam interface according to Equation (6). Therefore, a double-layer structure is formed on the HT9 steel. The process of oxidation is similar to that of the P92 steel in aerated supercritical water. The outer layer Fe_2O_3 and inner layer $(Fe, Cr)_3O_4$ grow at the oxide/steam and oxide/metal interface, respectively. The growth rates are controlled by the outward diffusion of Fe across the oxide layer.

$$2Cr + 3H_2O = Cr_2O_3 + 3H_2 \quad (2)$$

$$3Fe + 4H_2O = Fe_3O_4 + 4H_2 \quad (3)$$

$$Fe_3O_4 + 4H_2 = 3Fe + 4H_2O \quad (4)$$

$$Cr_2O_3 + Fe + H_2O = FeCr_2O_4 + H_2 \quad (5)$$

$$2Fe_3O_4 + H_2O = 3Fe_2O_3 + H_2 \quad (6)$$

Exfoliation of the oxide layer depends on the stress state and relative strength of the oxide and oxide/metal interface.[11] Crack initiation and crack propagation result in two different types of spallation. The oxidation layer exfoliates due to non-penetrating longitudinal cracks in the oxidation layer, or it humps and bends until it breaks and exfoliates due to interface cracks between the steel matrix and the oxidation layer.[22,23] A thicker oxide layer indicates a higher possibility of exfoliation for the oxide layer.[11,24]

Figure 8 shows the exfoliation of the oxide layers on the HT9 steel after exposure to steam. Some obvious exfoliation can be observed in the local areas of the oxide scale. The exfoliation of the oxide scale from the HT9 steel was probably due to the growth stress taking place when the oxide formed and grew on the specimens and the thermal stress due to the temperature variation caused by the difference in the thermal expansion coefficient between the oxides and the substrate.[25] If the oxide layer spalls at the interface between the inner and outer layers (**Figures 8a** to **8c**), the oxidation rate of the HT9 steel and the thickening rate of the oxide layer after exfoliation do not change substantially. The formation and growth of the oxide layer is still controlled by the diffusion of Fe and O through the inner layer. When the oxide layer exfoliates at the oxide/metal interface (**Figure 8b**), the oxidation rate of the steel becomes much higher than that before the oxide exfoliation. As can be seen in **Figure 8c**, the outer Fe_2O_3 layer was columnar. The oxide layer of the HT9 steel exposed to steam exfoliated by way of both non-penetrating longitudinal cracks and interface cracks penetrating the oxide scale.

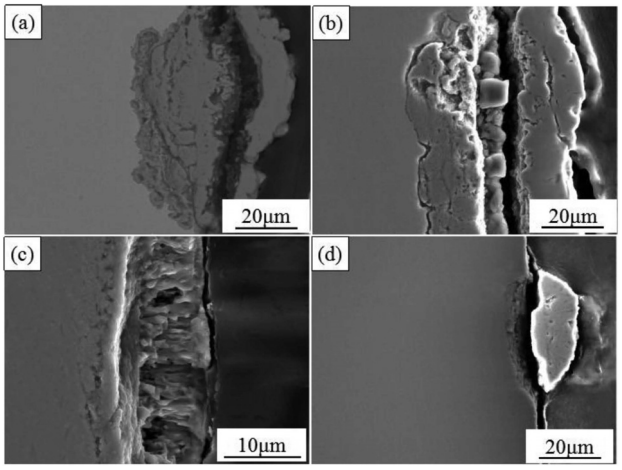

Figure 8: Exfoliation of the oxide scale formed on the HT9 steel in a steam environment: a) to b) 700 °C, 100 h, c) 800 °C, 20 h and d) 900 °C, 20 h

5 CONCLUSIONS

Steam oxidation behavior of the HT9 steel up to 100 h at 700–900 °C was investigated. The weight gain, phase constituents, morphologies and chemical compositions of oxide layers were investigated. It was found that the oxidation kinetics at (700, 800 and 900) °C followed the parabolic law and the mass gain increased with decreasing exposure temperatures. Double-layer oxides were produced on the steel, consisting of outer layer Fe_2O_3 and inner layer $(Fe, Cr)_3O_4$. Obvious cracks and exfoliation could be observed in the oxide scales. The formation and growth of the oxide layer can be explained with the diffusion of Fe and O. The oxide scales exfoliated due to non-penetrating longitudinal cracks and interface cracks penetrating the oxide scale.

Acknowledgment

This work was supported by National Natural Science Foundation of China, grant number 51575372 and the Fund for Shanxi Key Subject Construction.

6 REFERENCES

[1] O. Anderoglu, T. S. Byun, M. Toloczko, S. A. Maloy, Mechanical performance of ferritic martensitic steels for high dose applications in advanced nuclear reactors, Metall. Mater. Trans. A, 44 (**2013**), 70–83, doi:10.1007/s11661-012-1565-y

[2] C. Zheng, M. A. Auger, M. P. Moody, D. Kaoumi, Radiation induced segregation and precipitation behavior in self-ion irradiated ferritic/martensitic HT9 steel, J. Nucl. Mater., 491 (**2017**), 162–176, doi:10.1016/j.jnucmat.2017.04.040

[3] J. Bischoff, A. T. Motta, C. Eichfeld, R. J. Comstock, G. Cao, T. R. Allen, Corrosion of ferritic-martensitic steels in steam and supercritical water, J. Nucl. Mater., 441 (**2013**), 604–611, doi:10.1016/j.jnucmat.2012.09.037

[4] Y. R. Chen, Irradiation effects of HT-9 martensitic steel, Nucl. Eng. Tech., 45 (**2013**), 311–322, doi:10.5516/NET.07.2013.706

[5] L. Tan, M. T. Machut, K. Sridharan, T. R. Allen, Corrosion behavior of a ferritic/martensitic steel HCM12A exposed to harsh environments, J. Nucl. Mater., 371 (**2007**), 161–170, doi:10.1016/j.jnucmat.2007.05.001

[6] L. Tan, X. Ren, T. R. Allen, Corrosion behavior of 9–12% Cr ferritic–martensitic steels in supercritical water, Corros. Sci., 52 (**2010**), 1520–1528, doi:10.1016/j.corsci.2009.12.032

[7] J. H. Baek, T. S. Byun, S. A. Maloy, M. B. Toloczko, Investigation of temperature dependence of fracture toughness in high-dose HT9 steel using small-specimen reuse technique, J. Nucl. Mater., 444 (**2014**), 206–213, doi:10.1016/j.jnucmat.2013.09.029

[8] J. Żurek, E. Wessel, L. Niewolak, F. Schmitz, T. U. Kern, L. Singheiser, W. J. Quadakkers, Anomalous temperature dependence of oxidation kinetics during steam oxidation of ferritic steels in the temperature range 550–650 °C, Corros. Sci., 46 (**2004**), 2301–2317, doi:10.1016/j.corsci.2004.01.010

[9] P. J. Ennis, W. J. Quadakkers, Mechanisms of steam oxidation in high strength martensitic steels, Int. J. Pres. Ves. Pip., 84 (**2007**), 75–81, doi:10.1016/j.ijpvp.2006.09.007

[10] X. Zhong, X. Wu, E. H. Han, Effects of exposure temperature and time on corrosion behavior of a ferritic–martensitic steel P92 in aerated supercritical water, Corros. Sci., 90 (**2015**), 511–521, doi:10.1016/j.corsci.2014.10.022

[11] X. Zhong, X. Wu, E. H. Han, The characteristic of oxide scales on T91 tube after long-term service in an ultra-supercritical coal power plant, J. Supercrit. Fluid., 72 (**2012**), 68–77, doi:10.1016/j.supflu.2012.08.015

[12] N. Zhang, Z. Zhu, F. Lv, D. Jiang, H. Xu, Influence of exposure pressure on oxidation behavior of the ferritic–martensitic steel in steam and supercritical water, Oxid. Met., 86 (**2016**), 113–124, doi:10.1007/s11085-016-9624-1

[13] Q. Shi, J. Liu, H. Luan, Z. Yang, W. Wang, W. Yan, Y. Shan, K. Yang, Oxidation behavior of ferritic/martensitic steels in stagnant liquid LBE saturated by oxygen at 600 °C, J. Nucl. Mater., 457 (**2015**), 135–141, doi:10.1016/j.jnucmat.2014.11.018

[14] X. Ren, K. Sridharan, T. R. Allen, Corrosion of ferritic–martensitic steel HT9 in supercritical water, J. Nucl. Mater., 358 (**2006**), 227–234, doi:10.1016/j.jnucmat.2006.07.010

[15] Y. Chen, K. Sridharan, S. Ukai, T. R. Allen, Oxidation of 9Cr oxide dispersion strengthened steel exposed in supercritical water, J. Nucl. Mater., 371 (**2007**), 118–128, doi:10.1016/j.jnucmat.2007.05.018

[16] P. Ampornrat, G. S. Was, Oxidation of ferritic–martensitic alloys T91, HCM12A and HT-9 in supercritical water, J. Nucl. Mater., 371 (**2007**), 1–17, doi:10.1016/j.jnucmat.2007.05.023

[17] V. Lepingle, G. Louis, D. Allué, B. Lefebvre, B. Vandenberghe, Steam oxidation resistance of new 12%Cr steels: Comparison with some other ferritic steels, Corros. Sci., 50 (**2008**), 1011–1019, doi:10.1016/j.corsci.2007.11.033

[18] N. Q. Zhang, Z. L. Zhu, H. Xu, X. P. Mao, J. Li, Oxidation of ferritic and ferritic–martensitic steels in flowing and static supercritical water, Corros. Sci., 103 (**2016**), 124–131, doi:10.1016/j.corsci.2015.10.017

[19] T. Cheng, J. R. Keiser, M. P. Brady, K. A. Terrani, B. A. Pint, Oxidation of fuel cladding candidate materials in steam environments at high temperature and pressure, J. Nucl. Mater., 427 (**2012**), 396–400, doi:10.1016/j.jnucmat.2012.05.007

[20] L. Martinell, F. Balbaud-Célérier, A. Terlain, S. Delpech, G. Santarini, J. Favergeon, G. Moulin, M. Tabarant, G. Picard, Oxidation mechanism of a Fe–9Cr–1Mo steel by liquid Pb–Bi eutectic alloy (Part I), Corros. Sci., 50 (**2008**), 2523–2536, doi:10.1016/j.corsci.2008.06.050

[21] W. Gao, X. Guo, Z. Shen, L. Zhang, Corrosion behavior of oxide dispersion strengthened ferritic steels in supercritical water, J. Nucl. Mater., 486 (**2017**), 1–10, doi:10.1016/j.jnucmat.2017.01.014

[22] H. E. Evans, Stress effects in high temperature oxidation of metals, Metall. Rev., 40 (**1995**), 1–40, doi:10.1179/imr.1995.40.1.1

[23] H. E. Evans, Cracking and spalling of protective oxide layers, Mat. Sci. Eng. A, 120 (**1989**), 139–146, doi:10.1016/0921-5093(89)90731-4

[24] E. Essuman, G. H. Meier, J. Żurek, M. Hänsel, W. J. Quadakkers, The effect of water vapor on selective oxidation of Fe–Cr aloys, Oxid. Met., 69 (**2008**), 143–162, doi:10.1007/s11085-007-9090-x

[25] N. H. Lee, S. Kim, B. H. Choe, K. B. Yoon, D. I. Kwon, Failure analysis of a boiler tube in USC coal power plant, Eng. Fail. Anal., 16 (**2009**), 2031–2035, doi:10.1016/j.engfailanal.2008.12.006